Volume 18, Number 1, 2025. pp. 33-40

Jordan Journal of Physics

ARTICLE

Field Emission Characteristics of Carbon Black Particles and Various Types of Carbon Nanotubes Using Glass Tubes

Hatem A. Al-Braikat[a], **Samer I. Daradkeh**[b,c], **M-Ali H. Al-Akhras**[a] and **Marwan S. Mousa**[d]

[a] *Department of Physics, Jordan University of Science and Technology, Irbid, Jordan.*

[b] *Central European Institute of Technology, Brno University of Technology, Purkyňova 656/123, 612 00, Brno, Czech Republic.*

[c] *Department of Physics, Faculty of Electrical Engineering and Communication, Brno University of Technology, Technická 2848/8, 616 00, Brno, Czech Republic.*

[d] *Department of Renewable Energy, Jadara University, Irbid 21110, Jordan.*

Doi: **https://doi.org/10.47011/18.1.4**

Received on: 12/07/2023; *Accepted on: 26/01/2024*

Abstract: Carbon-based nanomaterials have gained considerable attention in recent decades owing to their exceptional structural and material characteristics, such as high thermal and electrical conductivity, chemical stability, and high aspect ratio. These remarkable properties make carbon-based nanomaterials highly desirable for various scientific and industrial applications. In this research, the field electron emission (FEE) properties of different materials were investigated using current-voltage (I-V) characteristics and the well-known Fowler-Nordheim (FN) plots. Specifically, four types of carbon-based nanomaterials were examined: single-walled carbon nanotubes (SWCNTs) synthesized through a high-pressure carbon monoxide process involving Fe particles, multi-walled carbon nanotubes (MWCNTs) with a carbon purity of 90% known as NanoclyTM NC 7000, carbon nanotube fibers (CNTFs) denoted as III PR-1, and carbon black (CB) referred to as Vulcan XC72. Field emission tips, also known as emitters, were fabricated using a glass-drawing technique, with the carbon material inserted until it protruded from the broken end. These emitters were then characterized using field emission microscopes (FEM) under ultra-high vacuum (UHV) conditions, with a cathode-to-screen (anode) separation of approximately 10 mm. The results obtained from the CB material exhibited satisfactory agreement with the linearity of the FN plots, while the other materials showed this agreement primarily at low applied voltages. The emission images appeared as a single-spot pattern at low voltages for SWCNTs and CNTFs, whereas CB and MWCNTs exhibited this characteristic pattern at higher voltages.

Keywords: Field emission, Fowler-Nordheim, Single-Walled carbon nanotubes, Multi-Walled carbon nanotubes, Carbon black, Carbon nanofibers.

1. Introduction

Electrons can be emitted from the surfaces of materials through several mechanisms, including thermionic emission, where the electrons gain sufficient thermal energy to overcome the potential barrier and extract into the vacuum or air. Photoelectric emission takes place when incident photons transfer energy to electrons, enabling them to surpass the material's work function threshold and emit from the surface. [1]. Cold field electron emission (CFE) represents a quantum mechanical phenomenon operating at high electric field strengths and low

Corresponding Author: Marwan S. Mousa **Email**: m.mousa@jadara.edu.jo

temperatures, wherein electrons with energies below the Fermi level are extracted through quantum tunneling across a narrowed potential barrier, without requiring the substantial energy input characteristic of other emission processes [2].

After 1922, CFE attracted more attention than thermionic emission due to its low energy spread, high brightness, and concentrated emission pattern [3]. Thermionic emission has a higher energy consumption, wider energy spread, and metal degradation caused by the high operating temperature [4]. Additionally, CFE can be operated at room temperature, which makes it more advantageous. CFE from cathodes can provide high current densities for a variety of applications, such as high-power microwave generation [5], vacuum electronics [6], X-ray generation [7], and space vehicle neutralization [8]. For electron extraction, the material must be subjected to a strong electric field, typically around $\sim 3\,\mathrm{V/m}$ [9]. To achieve optimal field emission performance, emitters must be fabricated with high-curvature apices, as these geometrical features effectively concentrate the electric field at the tip region. This field enhancement phenomenon significantly reduces the required applied voltage for electron extraction, improving operational efficiency. The concentrated electric field at these sharp tips creates localized regions of intense field strength, facilitating quantum tunneling by narrowing the potential barrier at the emission surface.

Extensive experimentation has been conducted on various metals and metal oxide materials, employing different emitter fabrication methods such as zinc oxide (ZnO), tungsten (W) nanowires, liquid metal (gallium-Ga), and more, in the field of cold field emission. However, due to the active nature of metals, the presence of residual gases, and ion bombardment during the field emission process, limitations arise in terms of emitter lifetime and fluctuations in field emission current [10], hindering the advancement of field emission. Consequently, researchers are actively seeking alternative materials that exhibit favorable characteristics for utilization as field emitters [11].

In 1889, carbon nanotube fibers (CNTFs III PR-1) were first discovered. Studies have reported the growth of carbon filaments from carbon-containing gases using a metallic crucible as the catalyst. Notably, Robertson [12] was among the first to observe that the interaction between methane and metal surfaces at relatively low temperatures resulted in the formation of graphitic carbon [13]. The accidental discovery of multiwalled carbon nanotubes (MWCNTs) occurred in 1991 when Iijima [14] was investigating the surfaces of a graphite electrode employed in electric arc discharge. Subsequently, in 1993, Iijima and his colleague discovered single-wall carbon nanotubes (SWCNTs) by identifying single-shell tubules within soot-like deposits formed in a carbon-arc chamber [15]. Carbon black (CB), similar to other colloidal materials generated in a flame, exists in the form of primary aggregates where the primary particles are fused [16]. It is well-established that carbon nanotubes (CNTs) can emit electrons at relatively low electric fields and can sustain a stable and intense current, aligning with the principles of the standard Fowler-Nordheim (FN) theory.

The unique structure of CNTs, including their high aspect ratio [17], high thermal and electrical properties [18], high chemical stability, and high melting point [19], are the reasons behind their superior performance in CFE from their surfaces. CFE, specifically from CNTs, is affected by a set of factors. These factors include ion bombardment (as mentioned before) and the existence of adsorbate on the surface, which sometimes can contribute to field emission, change emission current values, and could be identified as a sudden raise in the emission current value [20]. CNTs of different lengths and diameters with low vacuum can cause field emission fluctuations and the interaction between neighboring nanotubes [21], which can reduce the effective field enhancement factor [22]. Vacuum space charge can also lead to fluctuations in emission current [23]. Different techniques were conducted to mitigate the emission current fluctuation and improve overall field emission characteristics, for instance, high temperature annealing or heating of the tip by the extracted electron current for relatively long time can decrease defects of CNTs, thereby improving the efficiency of the emitter[24-25]. Additionally, the high aspect ratio can affect the field enhancement factor, thus improving the emitted current [26]. The existence of resistance in a CNT can cause the current to saturate [27], where the linear shape of the $(\mathrm{I}-\mathrm{V})$

characteristics can denote the existence of resistance. There are two positions where resistance can exist: one along the carbon nanotube/nanofibers (CNs) and the other at the CN/substrate interface [28].

In this study, the emitters were fabricated using a glass puller apparatus, employing a drawing technique [29]. CNT tips show a deviation from the FN theory, but CBs follow it. Also, all types form a single-spot pattern at a relatively low applied voltage except for CB, which showed a single-spot pattern at a high applied voltage value as well [30-31]. However, the theory is often applied in other situations.

The elementary Fowler-Nordheim (FN) type equation can be written as:

$$i = A_n\{a\phi^{-1}(\beta_v V)^2\}\exp[-b\phi^{-3/2}/\beta_v V] \quad (1)$$

This equation is utilized to depict the phenomenon of field emission. The equation includes several variables: emission current (i), local work function (ϕ), applied voltage (V), local voltage-to-surface field conversion factor at a reference point (β_v), and notional emission area (A_n). The constants a and b are the first and second Fowler-Nordheim (FN) constants [32]. In the FN plot, $\ln(I/V^2)$ is plotted on the y-axis and $1/V$ on the x-axis [33]. Ideally, the FN plot should be a straight line; however, deviations can occur, as evidenced by the multilinear segments observed in SWCNTs, MWCNTs, and CNTFs III PR-1 in the results and discussion section.

Using Eq. (1) to describe the FN mechanism in CNTs presents challenges due to factors such as wave function structure, band structure, and the effect of screened potential. These factors are more pronounced in small-radius emitters like CNTs [34]. CNTs differ from bulk materials, such as metals, in several ways [35–36], including their energy band structure and the influence of impurities and defects on electron emission [37]. For example, the presence of impurities and defects can generate localized states near the Fermi energy, altering the emitter's energy band structure. Furthermore, in single-walled carbon nanotubes (SWCNTs), the density of states near and above the charge neutrality level is lower than in metals [38]. As a result, field penetration and band bending effects can occur, particularly near the emitter apex, leading to local dipole effects [39]. Therefore, treating SWCNTs as bulk metals is not accurate [40–41].

This study investigates the field emission properties of carbon-based nanomaterials, emphasizing their potential for various scientific and industrial applications due to their distinctive structural and material characteristics. Additionally, it aims to contribute to ongoing research on identifying the optimal material and fabrication method for electron emitters by comparing the field electron emission (FEE) characteristics of several materials using common tools such as the I-V plot and the corresponding FN plot.

2. Materials and Methods

2.1 Materials

All materials were bought from specialized companies. The SWCNTs were produced via catalytic conversion of high-pressure CO over Fe particles (HiPCO) processed at CNI in Houston, TX. Individual SWCNTs have a length of approximately $1-3$ μm, a mean diameter of $1-4$ nm, and a surface area of $1040\ m^2/g$. MWCNTs (Nanocyl^{TM} NC7000 S.A., Belgium) were produced via chemical vapor deposition, with a diameter of 9.5 nm and a high aspect ratio (>150) [42]. The CNTFs Pyrograf III PR-1 have an average fiber diameter of $100-200$ nm and a length of $30-100$ μm. The CB Vulcan XC72 processed at CABOT Corporation has an average particle size of approximately 30 nm, with the mean size of primary aggregates ranging between 100 and 200 nm [43-44].

2.2 Methods

The emitters used in this study were fabricated using a glass puller device, employing a drawing technique as depicted in Fig. 1. In this process, carbon-based material was mechanically inserted into a glass tube, ensuring a consistent distribution along its length. The glass tube had an internal diameter of 0.1 mm and an external diameter of 1 mm, creating a controlled environment necessary for precise field emission measurements.

FIG. 1. Actual image of the glass puller, which heats and stretches glass tubes using gravity to create sharp emitter tips essential for producing the high electric field required in field emission.

The glass puller plays a pivotal role in this method by creating sharp emitter tips, which are essential for achieving the high electric field required for field emission. This technique allows for reproducible and well-defined tips that significantly influence the onset and behavior of the field emission. The precise geometry of the emitter tip is critical in reducing the threshold voltage and ensuring consistent emission characteristics. Further details on the emitter preparation and the operation of the glass puller can be found in prior works [45]. The uniformity of the emitter preparation ensures reliable and accurate measurements of the field emission properties, which are essential for understanding the performance of the materials being studied.

Field emission efficiency (FEE) measurements were conducted using a field emission microscope (FEM) within a high-vacuum chamber, which was evacuated to a base pressure of approximately 10^{-7} mbar. To remove any residual contaminants that might affect the measurements, the chamber was baked overnight at 180°C. The distance between the emitter and screen was maintained at approximately 10 mm, providing optimal conditions for accurate field emission measurements. The FEM system was connected to a 100 MΩ current-limiting resistor, which was essential for protecting the system from excessive current during the emission process. The testing began by gradually increasing the applied voltage, at which point the "switch-on" phenomenon occurred. This was marked by a rapid increase in the emission current, transitioning from the nanoampere (nA) to the microampere (μA) range. At this point, the emission current, denoted as I_{SW}, and the corresponding voltage, V_{SW}, were recorded. The "switch-on" phenomenon is an important feature of field emission as it signifies the point at which emission begins. As the applied voltage decreased, a constant resistance regime was observed, during which the emission current remained stable until the voltage reached a specific value, V_C. The corresponding current in this regime, denoted as I_C, reflects the emitter's stable behavior under reduced voltage. Further reduction of the applied voltage led to a gradual decrease in emission current, eventually reaching a threshold voltage, V_{TH}, where the emission current fell to zero [46]. The current at this voltage, denoted I_{TH}, represents the point at which the emitter stops contributing to the current flow. This detailed characterization of the emission process, including the "switch-on" behavior, constant resistance regime, and threshold voltage, provides valuable insight into the emission properties and efficiency of the materials under investigation. Understanding these parameters is crucial for evaluating the potential of carbon-based materials in field emission applications [47].

3. Results and Discussion

The most common approach to presenting data from field emission experiments involves current-voltage (I-V) plots and their corresponding Fowler-Nordheim (FN) plots, where $\ln(1/V^2)$ is plotted on the y-axis and $1/V$ on the x-axis. During the experiments, emission current images were captured using a digital camera. All samples were tested under identical conditions of pressure and emitter-screen distance. Table 1 summarizes the switch-on voltage (V_{SW}) and threshold voltage (V_{TH}) values for all samples.

TABLE 1. The values of V_{SW}, I_{SW}; V_C, I_C; and V_{TH}, I_{TH} for all samples.

SWCNTs	V_{SW}, I_{SW} = 700 V, 3.05 μA	V_C, I_C = 450 V, 1.1 μA	V_{TH}, I_{TH} = 140 V, 4.2 pA
MWCNTs	V_{SW}, I_{SW} = 3500 V, 16 μA	V_{SAT}, I_{SAT} = 1600 V, 2.9 μA	V_{TH}, I_{TH} = 600 V, 9.6 pA
CNTFs	V_{SW}, I_{SW} = 750 V, 3.6 μA	V_C, I_C = 350 V, 1.09 μA	V_{TH}, I_{TH} = 140 V, 10 pA
CB	V_{SW}, I_{SW} = 4450 V, 1.1 μA	V_{SAT}, I_{SAT} = 4400 V, 1.4 μA	V_{TH}, I_{TH} = 4000 V, 6 pA

Field electron emission was initiated at relatively lower applied voltages for SWCNTs and CNTFs III PR-1 compared to CBs and MWCNTs The latter materials demonstrated higher voltage requirements for comparable emission performance, indicating superior field enhancement characteristics in the SWCNT and CNTF structures. Additionally, SWCNTs exhibited a broader saturation region, extending to lower voltage values than MWCNTs and CBs. A similar trend was observed for the switch-on phenomenon, which occurred at lower voltages for SWCNTs.

The SWCNT emitter demonstrated the earliest "switch-on" phenomenon at the lowest applied voltage among all emitters, highlighting its superior performance in initiating electron emission. In contrast, the CNTFs III PR-1 emitter exhibited a saturation region extending to even lower voltage values than the SWCNT emitter, indicating distinct differences in their emission characteristics.

For the SWCNTs emitter, as the applied voltage gradually increased, the emission current began at 320 V with 4.2 pA and rose steadily until the "switch-on" event occurred at 700 V, producing 3.05 µA. The emission current continued to rise with increasing voltage, peaking at 6.2 µA at 1050 V. Upon reducing the voltage, a constant-resistance regime persisted until 450 V, where a regime change occurred, corresponding to an emission current of 1.1 µA. Further voltage reduction led to a gradual cessation of emission at 140 V and 4.2 pA. The linear current-voltage behavior can be attributed to significant resistance within the circuit, likely at the CNT interface, which also contributes to deviations in the FN plot's shape. Voltage drops in the circuit likely influence electron energy distribution, altering emission characteristics, as shown in Figs. 2(A) and 2(B).

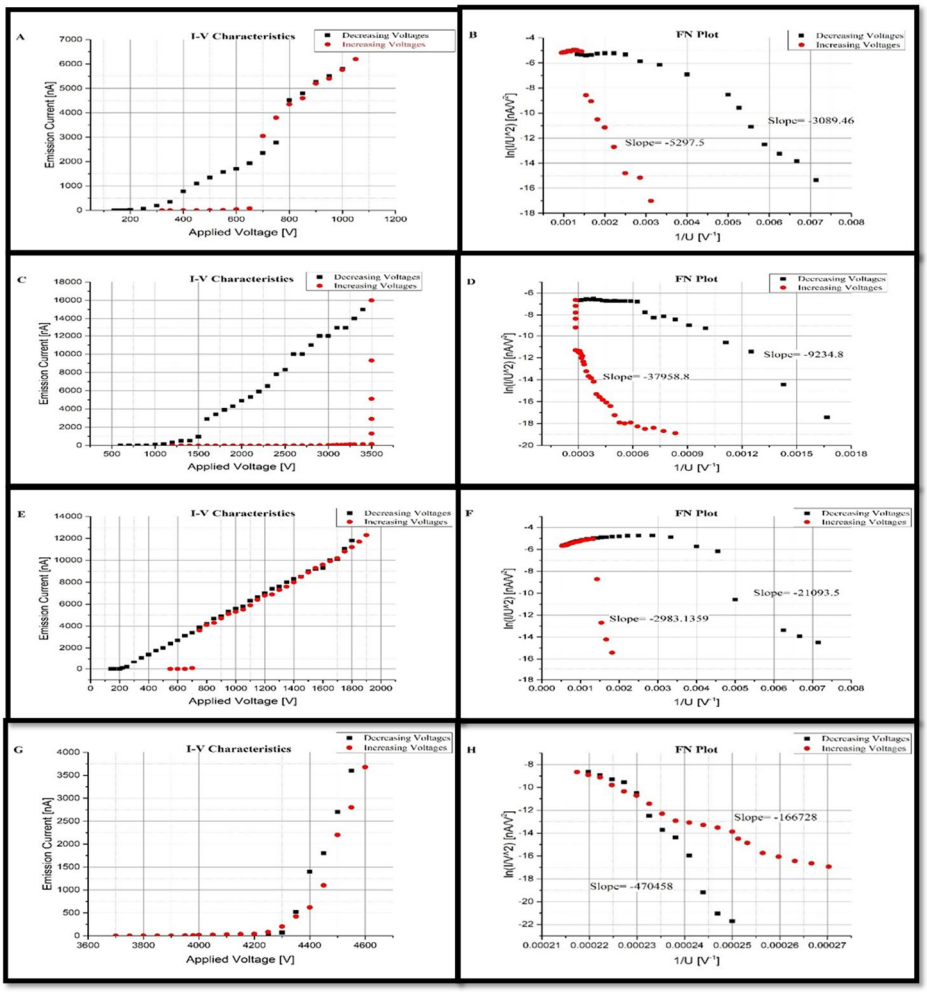

FIG. 2. the I-V characteristics for all the emitters employed in the experiment, with its related F-N plots, where (A) and (B) for the SWCNTs, (C) and (D) for MWCNTs, (E) and (F) for CNTFs III PR-1, and (G) and (H) for the CB. (B), (D), and (F): The non-linear shape of the FN plot for CNTs, where the slope in the high-field region is much lower than that in the low-field regime.

For the MWCNTs emitter, the voltage range spanned from 1200 to 3500 V, with emission currents from 9.1 pA to 1.3 μA. The "switch-on" phenomenon occurred at 3500 V, yielding an emission current of 16 μA. Notable jumps in current, potentially due to activation of new emission sites or adsorbate contributions, were observed as shown in Figs. 2(C) and 2(D). The saturation region extended down to 1600 V, with a saturation current of 2.9 μA. Upon further voltage reduction, the emission current ceased at 600 V with 9.6 pA.

A comparison between the MWCNTs and CNTFs emitters revealed that CNTFs initiated emission at a much lower voltage (750 V vs. 3500 V for MWCNTs), with a consistent-resistance regime indicating stable performance, as shown in Figs. 2(E) and 2(F). However, MWCNTs demonstrated higher emission currents at higher applied voltages, reflecting their capacity for greater emission under optimal conditions.

For the CBs emitter [see Figs. 2(G) and 2(H)], electron emission began at 3700 V with a current of 600 pA, rising to 3.68 μA at 4600 V. During voltage reduction, the emission current persisted in the microampere range down to 4400 V (1.4 μA), then declined to zero at 4000 V (6 pA). Unlike the CNT-based emitters, the CB emitter showed minimal evidence of a constant-resistance regime and exhibited a smaller emission pattern, likely due to surface instability caused by weak intermolecular forces.

The FN plot for the CB emitter displayed linearity, whereas the CNT emitters showed deviations, likely due to contact resistance. Field enhancement factors are also influenced by preparation methods. Vertically aligned CNTs exhibit higher field enhancement factors due to their optimal geometry, while randomly oriented CNTs experience screening effects and lower efficiency [48].

The emission current profile for all samples formed relatively focused spatial distributions, as shown in Figs. 3 and 4. Among the samples, CB emitters exhibited the smallest emission pattern, likely due to their spherical morphology.

These findings highlight the importance of emitter structure and preparation in optimizing field emission performance. Further investigations aim to leverage these properties for developing reliable electron sources.

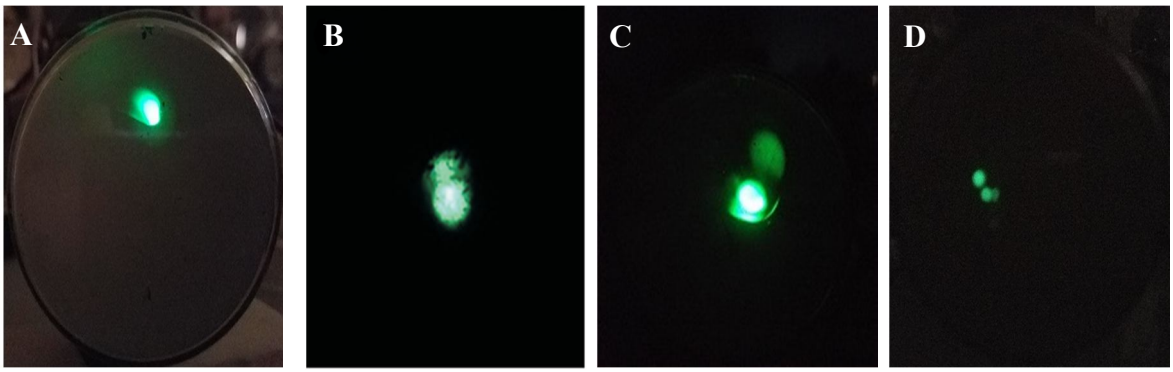

FIG. 3. Emission current images for (A) SWCNTs at 700 V, 2.35 μA. (B) MWCNTs at 3500 V, 0.15 μA. (C) CNTFs at 1300 V, 7.3 μA. (D) CB at 4600 V, 3.68 μA.

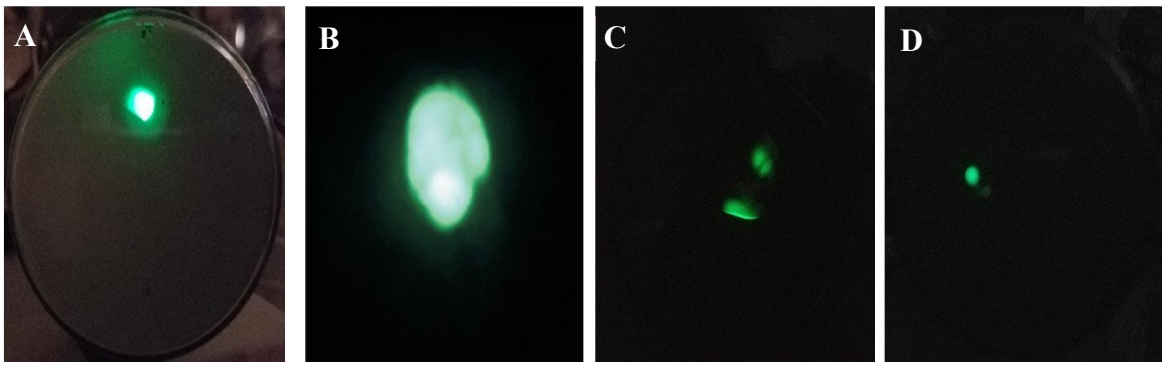

FIG. 4. Emission current for (A) SWCNTs at 900 V, 5.26 μA. (B) MWCNTs at 3500 V, 2.9 μA. (C) CNTFs at 950 V,5.1 μA. (D) CBs at 4400 V, 1.4 μA.

4. Conclusions

The emitters were prepared using a drawing technique with a glass puller. The CB emitter exhibits linear behavior in the FN plot and shows no obvious signs of series resistance, whereas such resistance was observed in the (I-V) plots for SWCNTs, MWCNTs, and CNTFs. The CNT emitters deviate from the linearity of the FN plot, possibly due to contact resistance, as indicated by the linear behavior of the (I-V) plot.

The emission current was initiated at a relatively low applied voltage for SWCNTs and CNTFs III PR-1, while CBs and MWCNTs required a higher applied voltage. Additionally, a saturation region was reported for the SWCNTs, extending to a lower voltage value than MWCNTs and CBs. The same situation has been recorded with the switch-on phenomenon, which occurs at lower applied voltage values. The emission current spatial pattern for all samples was approximately focused. CB emitters exhibited the smallest emitted current pattern, possibly due to the spherical structure of their particles.

This study focused on understanding the field emission behavior of different carbon-based materials—SWCNTs, MWCNTs, CNTFs, and CBs—to explore their potential as advanced electron sources. By comparing their performance under identical experimental conditions, we aimed to reveal how factors such as material properties, structure, and preparation methods influence key emission parameters, including switch-on voltage and saturation behavior. This research is driven by the need to optimize field emission performance and harness the unique properties of these materials to develop efficient and reliable electron sources for a wide range of applications in science and industry.

References

[1] Fischer, T.E., Phys. Rev., 142 (2) (1966) 519.

[2] Lu, X., Yang, Q., Xiao, C., and Hirose, A., J. Phys. D Appl. Phys., 39 (15) (2006) 3375.

[3] Shao, X. and Khursheed, A., Appl. Sci., 8 (6) (2008) 15.

[4] Giubileo, F., Di Bartolomeo, A., Iemmo, L., Luongo, G., and Urban, F., Appl. Sci., 8 (4) (2018) 526.

[5] Booske, J.H., He, X., Miller, R.L., Morgan, D., Scharer, J.E., Vlahos, V., Gilgenbach, R.M., Jordan, N.M., Lau, Y.Y., Feng, Y., and Verboncoeur, J., IEEE 34th International Conference on Plasma Science (ICOPS), (2007), 481.

[6] Gaertner, G., J. Vac. Sci. Technol. B, 30 (6) (2012) 060801.

[7] Yue, G.Z., Qiu, Q., Gao, B., Cheng, Y., Zhang, J., Shimoda, H., Chang, S., Lu, J.P., and Zhou, O., Appl. Phys. Lett., 81 (2) (2002) 355.

[8] Grandal, B. and North, A., "Artificial Particle Beams in Space Plasma Studies" (Springer US, 2012).

[9] de Heer, W.A., Châtelain, A., and Ugarte, D., Science, 270 (5239) (1995) 1179.

[10] Hideo, T., Norio, S., and Shigehiko, Y., Jpn. J. Appl. Phys., 21 (10R) (1982) 1513.

[11] Yunhan, L., Yonghai, S., and Yeow, J.T.W., Nanotechnology, 26 (24) (2015) 242001.

[12] Robertson, S.D., Nature, 221 (1969) 1044.

[13] De Jong, K.P. and Geus, J.W., Catal. Rev., 42 (4) (2000) 481.

[14] Iijima, S., Nature, 354 (6348) (1991) 56.

[15] Iijima, S. and Ichihashi, T., Nature, 363 (6430) (1993) 603.

[16] Medalia, A.I. and Heckman, F.A., Carbon, 7 (5) (1969) 567.

[17] Harris, P.J.F., "Carbon Nanotube Science: Synthesis, Properties and Applications" (Cambridge University Press, 2009).

[18] Hone, J., Llaguno, M.C., Nemes, N.M., Johnson, A.T., Fischer, J.E., Walters, D.A., Casavant, M.J., Schmidt, J., and Smalley, R.E., Appl. Phys. Lett., 77 (5) (2000) 666.

[19] Wei, X., Wang, M.-S., Bando, Y., and Golberg, D., Sci. Technol. Adv. Mat., 12 (4) (2011) 044605.

[20] de Jonge, N., Allioux, M., Oostveen, J.T., Teo, K.B.K., and Milne, W.I., Appl. Phys. Lett., 87 (13) (2005) 133118.

[21] Collins, P.G. and Zettl, A., Phys. Rev. B, 55 (15) (1997) 9391.

[22] Bonard, J.-M., Dean, K.A., Coll, B.F., and Klinke, C., Phys. Rev. Lett., 89 (19) (2002) 197602.

[23] Barbour, J.P., Dolan, W.W., Trolan, J.K., Martin, E.E., and Dyke, W.P., Phys. Rev., 92 (1) (1953) 45.

[24] Sun, Y., Shin, D.H., Yun, K.N., Hwang, Y.M., Song, Y., Leti, G., Jeon, S.-G., Kim, J.-I., Saito, Y., and Lee, C.J., AIP Adv., 4 (7) (2014) 077110.

[25] Schwoebel, P.R., Spindt, C.A., Holland, C.E., and Panitz, J.A., J. Vac. Sci. Technol., 19 (3) (2001) 980.

[26] Edgcombe, C.J. and Valdrè, U., J. Microsc., 203 (2) (2001) 188.

[27] Jo, S.H., Tu, Y., Huang, Z.P., Carnahan, D.L., Huang, J.Y., Wang, D.Z., and Ren, Z.F., Appl. Phys. Lett., 84 (3) (2004) 413.

[28] Minoux, E., Groening, O., Teo, K.B.K.., Dalal, S.H., Gangloff, L., Schnell, J.-P., Hudanski, L., Bu, I.Y.Y., Vincent, P., Legagneux, P., Amaratunga, G.A.J., and Milne, W.I., Nano Lett., 5 (11) (2005) 2135.

[29] Mousa, M.S., J. Phys. Conf. Ser., 305 (1) (2018) 012025.

[30] Kleshch, V.I., Purcell, S.T., and Obraztsov, A.N., Sci. Rep., 6 (2016) 35260.

[31] Baskin, L.M., Lvov, O I., and Fursey, G.N., Phys. Status Solidi B, 47 (1) (1971) 49.

[32] Peng, J., Li, Z., He, C., Chen, G., Wang, W., Deng, S., Xu, N., Zheng, X., Chen, G., Edgcombe, C.J., and Forbes, R.G., J. Appl. Phys., 104 (1) (2008) 014310.

[33] Forbes, R.G., Deane, J.H.B., Fischer, A., and Mousa, M.S., Jordan J. Phys., 8 (3) (2015) 125.

[34] Forbes, R.G., J. Vac. Sci. Technol. B, 28 (2) (2010) C2A43.

[35] Abuamr, A.M., Mousa, M.S., Al-Bashaish, S.R., Madanat, M.A., AlSoud, A., MD, A., and Sobola, D., Physica Scripta, 99 (10) (2024) 105029.

[36] Mousa, M. and Abuamr, A., Jordan J. Phys., 16 (2) (2023) 247.

[37] Chen, L.F., Song, H., Cao, L.Z., Jiang, H., Li, D.B., Guo, W.G., Liu, X., Zhao, H.F., and Li, Z.M., J. Appl. Phys., 106 (3) (2009) 033703.

[38] Liang, S.-D., "Quantum Tunneling and Field Electron Emission Theories" (World Scientific Publishign Co. Pte Ltd Singapore, 2014).

[39] Peng, J., Li, Z., He, C., Chen, G., Wang, W., Deng, S., Xu, N., Zheng, X., Chen, G., Edgcombe, C.J., and Forbes, R.G., J. Appl. Phys., 104 (1) (2008) 014310.

[40] Chen, Y., Shaw, D.T., and Guo, L., Appl. Phys. Lett., 76 (17) (2000) 2469.

[41] Wang, Y.H., Lin, J., and Huan, C.H.A., Thin Solid Films, 405 (1) (2002) 243.

[42] Wang, X.Q., Wang, M., Li, Z.H., Xu, Y.B., and He, P.M., Ultramicroscopy, 102 (3) (2005) 181.

[43] Hom, S., Bhattacharyya, A.R., Khare, R.A., Kulkarni, A.R., Saroop, M., and Biswas, A., J. Appl. Polym. Sci., 112 (2) (2009) 998.

[44] Mdarhri, A., Brosseau, C., and Carmona, F., J. Appl. Phys., 101 (8) (2007) 084111.

[45] Daradkeh, S.I. and Mousa, M.S., Appl. Microsc., 47 (3) (2017) 86.

[46] Al-Qudah, A.A., Mousa, M., and Fischer, A., IOP Conf. Ser., Mater. Sci. Eng., 92 (1) (2015) 012021.

[47] Yeong, K.S. and Thong, J.T.L., Appl. Surf., 233 (1-4) (2004) 20.

[48] Li, N., Yan, F., Pang, S., Chen, L., Jin, D., Xiang, W., Zhang, D., Dai, J., and Zeng, B., J. Korean Phys. Soc., 66 (2015) 1186.4.